

Numerical simulation of benzene transport in shoreline groundwater affected by tides under different conditions

Mahsa Kheirandish¹, Chunjiang An (✉)¹, Zhi Chen¹, Xiaolong Geng², Michel Boufadel²

¹ Department of Building, Civil and Environmental Engineering, Concordia University, Montreal, QC H3G 1M8, Canada
² Center for Natural Resources, Department of Civil and Environmental Engineering, New Jersey Institute of Technology, Newark NJ 07102, USA

HIGHLIGHTS

- An approach for assessing the transport of benzene on the beach was proposed.
- The behavior of benzene in the subsurface of the beach was impacted by tide.
- Tidal amplitude influenced the travel speed and the benzene biodegradation.
- Hydraulic conductivity had the impact on plume residence time and biodegradation.
- Plume dispersed and concentration decreased due to high longitudinal dispersivity.

ARTICLE INFO

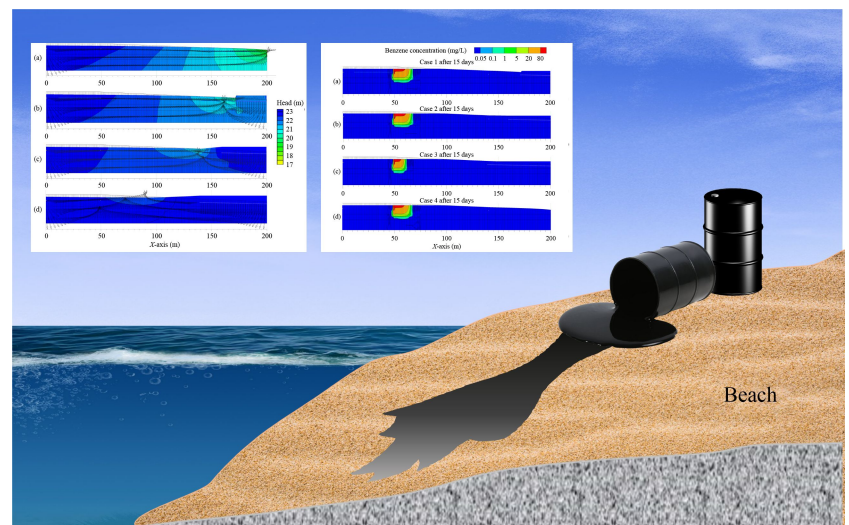
Article history:

Received 24 May 2021
Revised 6 January 2022
Accepted 16 January 2022
Available online 4 March 2022

Keywords:

Numerical simulation
Benzene
Transport and fate
Shoreline
Groundwater
Tide

GRAPHIC ABSTRACT



ABSTRACT

The release and transport of benzene in coastal aquifers were investigated in the present study. Numerical simulations were implemented using the SEAM3D, coupled with GMS, to study the behavior of benzene in the subsurface of tidally influenced beaches. The transport and fate of the benzene plume were simulated, considering advection, dispersion, sorption, biodegradation, and dissolution on the beach. Different tide amplitudes, aquifer characteristics, and pollutant release locations were studied. It was found that the tide amplitude, hydraulic conductivity, and longitudinal dispersivity were the primary factors affecting the fate and transport of benzene. The tidal amplitude influenced the transport speed and percentage of biodegradation of benzene plume in the beach. A high tidal range reduced the spreading area and enhanced the rate of benzene biodegradation. Hydraulic conductivity had an impact on plume residence time and the percentage of contaminant biodegradation. Lower hydraulic conductivity induced longer residence time in each beach portion and a higher percentage of biodegradation on the beach. The plume dispersed and the concentration decreased due to high longitudinal dispersivity. The results can be used to support future risk assessment and management for the shorelines impacted by spill and leaking accidents. Modeling the heterogeneous beach aquifer subjected to tides can also be further explored in the future study.

© Higher Education Press 2022

1 Introduction

Unexpected discharges of organic pollutants have had an increasing effect on coastal aquifers in recent decades

✉ Corresponding author
E-mail: chunjiang.an@concordia.ca

(Zhao et al., 2019; Chen et al., 2020; Li et al., 2021; Wang et al., 2021). Pollutants released from petrol stations, pipelines, and industrial activity, for instance, have a detrimental effect on shoreline groundwater (Lee et al., 2015; Boufadel et al., 2016). Such subsurface pollution may further affect the coastal ecosystem and its inhabitants. To evaluate and remediate subsurface contamination, however, a deeper understanding of the status and transport mechanism of pollutants in groundwater is critical (Colombani et al., 2015; Liu et al., 2016). In coastal aquifers, due to the complex mechanisms underlying groundwater flow (e.g., tide, waves, dissolved solutes), identifying the residence time, fate, and natural degradation of the plume is a challenge (Heiss and Michael, 2014; Geng et al., 2017).

Various studies have been carried out to investigate the behavior of groundwater and the plume transport in coastal aquifers (Robinson et al., 2007; Santos et al., 2012). Several factors have been identified as affecting subsurface flow pathways and solute transport. For instance, tides can recirculate groundwater and seawater on the oceanic side of aquifers, making them a critical oceanic force (Heiss, 2011; Geng et al., 2020b). Oil discharged to groundwater undergoes various processes that modify its structure and concentration. These chemical, physical, and biological processes have a significant impact on the toxicity and permanence of the pollution (Liu et al., 2012; Bi et al., 2020). Various physical remediation strategies have been applied in response to oil spills to eliminate or disperse oil in order to mitigate its harmful effect on the environment. Microbial degradation, meanwhile, is a biological process that can be applied to clean up petroleum hydrocarbon contamination (Leahy and Colwell, 1990; Atlas and Hazen, 2011; Jiang et al., 2019). In the biodegradation process, petroleum hydrocarbons are typically electron donors. The electron acceptors vary from oxygen (O_2) to sulfate (SO_4^{2-}), nitrate (NO_3^-), ferric ions (Fe(III)), oxidized manganese (Mn(IV)), and carbon dioxide (CO_2). Microbes use the energy released from this redox reaction for microbial growth.

Due to the restriction of field experiments and lack of experimental data, numerical simulation is often used as a good supplement for investigating the pollutant transport and fate (Geng et al., 2020a; Zhai et al., 2020b; Babamiri et al., 2021). A number of numerical models have been introduced by researchers based on particular field situations. Uraizee et al. (1997) constructed a mathematical model that considered the relationship between the biodegradation of crude oil and the bioavailability parameter. A two-dimensional model was developed by Boufadel et al. (1999) to estimate the solute in relation to water density and viscosity using the MARUN model. Essaid et al. (2003) quantified BTEX (benzene, toluene, ethylbenzene and xylene) dissolution and biodegradation of crude oil using the BIOMOC code combined with the

UCODE. The inverse modeling incorporating transport and degradation processes as well as a single dissolution rate coefficient was proposed to study a complex system. Li and Boufadel (2010) conducted two-dimensional variable density and saturation simulations using the MARUN model to assess the durability of the oil. Torlapati and Boufadel (2014) applied the numerical model, BIOB, to simulate the biodegradation of oil captured in sediment. Based on Monod kinetics, this model can analyze the bacteria growth considering nutrient presence and hydrocarbon consumption. Xu et al. (2015) predicted the fate of spilled gasoline in soil and groundwater using the Hydrocarbon Spill Screening Model (HSSM) coupled with the modified Modular Three-Dimensional Multispecies Transport Model (MT3DMS). HSSM was used to simulate the gasoline migration in vadose zone and the benzene dissolution in oil lens, and the modified MT3DMS was used to predict the transport and biodegradation of dissolved benzene in groundwater. Although these works are encouraging, knowledge of the fate and transport of petroleum pollutants in shoreline groundwater remains limited. The impacts of some shoreline conditions, such as tide, are not clear.

Benzene is a natural component of crude oil, and it has been identified as a lethal chemical that can cause acute and chronic poisoning. Benzene is a low molecular weight aromatic that has a comparatively high solubility in water (Lu et al., 1999; Brovelli et al., 2007; Sbarbati et al., 2015). In this context, the objectives underlying the research presented in this paper are (a) to use the numerical model SEAM3D (Sequential Electron Acceptor Model, 3 Dimensional) coupled with GMS (Groundwater Modeling System) as a reactive transport model to simulate transport, fate, and complex biodegradation processes involving benzene and different electron acceptors (e.g., oxygen and nitrate); and (b) to identify the key factors influencing a pollution plume's fate in shorelines, such as tide amplitude and beach properties (i.e., hydraulic conductivity and longitudinal dispersivity).

2 Methods

2.1 GMS models

Environmental simulation is an important approach for investigating the transport and fate of pollutants (Asif and Chen, 2020; He et al., 2020; Zhai et al., 2020a). In the present study, numerical models are used to investigate and evaluate the validity of various studies available in the literature concerning (i) the situation and nature of flow-system boundaries; (ii) recharge and discharge locations; and (iii) the hydrogeological framework. MODFLOW-2000 is a three-dimensional saturated

groundwater flow model, and SEAM3D is a tool for modeling three-dimensional solute transport coupled with aerobic and sequential anaerobic biodegradation and dissolution of non-aqueous phase liquid (NAPL). Both of them are available in GMS software (Aquaveo; USA). In the present study, hydraulic heads and cell-by-cell fluxes were estimated using the MODFLOW model, while the flow simulation and SEAM3D were applied to model multiple solutes in a three-dimensional, anisotropic, heterogeneous aquifer subject to advection, dispersion, sorption, and biodegradation. These two models were implemented in a two-step (flow and transport) simulation following the GMS.

MODFLOW, a finite-difference code coupled in the GMS, was applied in order to develop a steady- and unsteady-state groundwater flow model (Mehl and Hill, 2001). The three-dimensional flow of a subsurface of uniform density through porous ground, it should be noted, can be characterized using the following partial differential equation:

$$\frac{\partial}{\partial x} \left(K_x \frac{\partial h}{\partial x} \right) + \frac{\partial}{\partial y} \left(K_y \frac{\partial h}{\partial y} \right) + \frac{\partial}{\partial z} \left(K_z \frac{\partial h}{\partial z} \right) + W = S_s \frac{\partial h}{\partial t} \quad (1)$$

where K_x, K_y , and K_z represent hydraulic conductivity along the x, y , and z axes, respectively; h is the hydraulic head; W represents sources and sinks of water (the volumetric flux per unit of volume); S_s represents the specific storage; and t is time. This equation is used to demonstrate the groundwater flow of the non-equilibrium state in heterogeneous and anisotropic soil. To achieve approximate solutions of this equation, numerical schemes such as the finite-difference method are applied based on the discretization of points in time and space (Anderson et al., 2015).

The advection-dispersion equation is employed to describe the aqueous phase transport of all biodegradable substrates, electron acceptors, final products, mineral nutrients, and nonbiodegradable solutes. Equation (2) demonstrates the 3D transport of contaminants in groundwater:

$$\begin{aligned} & -\frac{\partial}{\partial x_i} (v_i S_{ls}) + \frac{\partial}{\partial x_i} \left(D_{ij} \frac{\partial S_{ls}}{\partial x_j} \right) + \frac{q_s}{\theta} S_{ls}^* - R_{\text{sink},ls}^{\text{bio}} + R_{\text{source},ls}^{\text{NAPL}} \\ & = R_{ls} \frac{\partial S_{ls}}{\partial t} \end{aligned} \quad (2)$$

where S_{ls} is the aqueous phase substrate concentration [$M_{ls}L^{-3}$] for $ls = 1, 2, \dots, NS$ (number of substrates); S_{ls}^* is the substrate point source concentration [$M_{ls}L^{-3}$]; v_i is the average pore water velocity [LT^{-1}]; x_i is the distance [L]; D_{ij} is the tensor for the hydrodynamic dispersion coefficient [L^2T^{-1}]; $R_{\text{sink},ls}^{\text{bio}}$ is the substrate biodegradation sink term [$M_{ls}L^{-3}T^{-1}$]; $R_{\text{source},ls}^{\text{NAPL}}$ is the substrate source term due to NAPL dissolution [$M_{ls}L^{-3}T^{-1}$]; R_{ls} is the retardation factor for substrate ls [L^0]; t is time [T]; θ is aquifer porosity [L^0]; and q_s is the volumetric flux of water per unit volume of the aquifer [T^{-1}] with $q_s > 0$ for

sources and $q_s < 0$ for sinks. In the case of a point sink, the concentration is generally not specified, and the model uses $S_{ls}^* = S_{ls}$ (Widdowson et al., 1988). The model follows Monod kinetics for the biodegradation of each substrate. The effects of electron acceptors and nutrient availability, inhibition, and threshold concentration are also considered.

2.2 Numerical implementation

The domain of the flow and transport model is 200 m long with a slope of 4% (i.e., 200 cells) in the x -direction (domain length), 10 m (i.e., 10 cells) in the y -direction (domain width), and 25 m (i.e., 3 layers) in the z -direction (domain depth), as shown in Fig. 1. The cells are 1 m long and 1 m wide. In the present study, the deepest layer is 10 m thick, while the middle layer is 5 m thick, and the top elevation of this layer is 15 m. Meanwhile, the top elevation of the surface layer is 25 m on the shoreline side, and, due to the slope, about 19 m on the seaside (the thickness changed from 10 to 4 m). However, the upper layer's hydraulic head changes with time (different tide levels), resulting in transient sea-side boundary conditions governed by the tides. The inland head is about 23 m (2 m below the beach surface), and the sea-side head is about 19 m in the no-tide state, while it ranges from 22 to 24 m under different tide conditions. The cosine function is approximated for the tide on the seaside, as follows:

$$H_{\text{tide}} = H_0 + A \cos \omega t \quad (3)$$

where H_0 is the average sea level ($H = 21$ m); A is the tide amplitude ($A = 1, 2$, or 3 m); ω is the tidal angular frequency ($\omega = 0.26$ rad/h); and t is the tidal period. The density difference between salty coastal water and fresh groundwater is an essential component for most aquifer systems, while there are various scenarios in which density effects are negligible. Based on different tracers, like an isotopic compound of Cl and Sr, deep saline water exists for some shoreline groundwater (Khaska et al., 2013). In the present study, the density effect was not significant for the mixing simulation.

The domain characteristics (e.g., hydraulic conductivity and longitudinal dispersivity) and the boundary inputs to the model to simulate the transport and fate of the benzene, nutrients, and oxygen were obtained from the study of Geng et al. (2015) for a tidally affected seashore in the Gulf of Mexico. The concentration of nitrate was found to be 1.2 mg-N/L on the shoreline and 0.2 mg-N/L on the seaside. The overall oxygen concentration in the whole area under consideration was 8.2 mg/L. It was assumed that the benzene was released into the shoreline accidentally through the point source (1 m \times 10 m landfill) positioned at $x = 50$ m, which is 110 m away from the sea side. The contaminant release period was 15 d at a benzene concentration of 100 mg/L (Geng et al.,

2017). The parameters of microbial kinetics applied in simulating the biodegradation of benzene were obtained from Chen et al. (1992), Essaid et al. (1995), and El-Kadi (2001). The values of these parameters were assumed to be uniform in all layers of the aquifer in the three-dimensional model. The concentrations of aerobes and nitrate reducers at the outset of the simulation were consistent throughout the aquifer. The starting biomass of aerobes was higher than that of the nitrate reducers, given the theory that aerobic biomass will predominate when the domain has a significant oxygen level under primary conditions. The aerobic biomass of 5 g/m^3 corresponded to $16.6 \times 10^6 \text{ cells/cm}^3$, assuming a cell volume of $1 \mu\text{m}^3$, cell density of 1.0 g/cm^3 . Therefore, the high amount of aerobic maximum utilization rate and the quantity of the cell's permissive considerable aerobic uptake of hydrocarbon substrates occur instantly. However, anaerobic microbes can only survive in anaerobic microenvironments if they are inside soil aggregates (Brook et al., 2003). Hence, the nitrate reducer concentrations were a magnitude lower than the aerobic biomass concentrations.

The yield coefficients were applied in the model to determine the theoretical microbe growth resulting from the degradation of hydrocarbon substrates. As per the calculations reported by Bailey and Ollis (1986), the stoichiometric coefficient for oxygen utilization based on complete mineralization was set to $3.47 \text{ mg of O}_2/\text{mg}$ of substrate. The yield coefficient for oxygen and nitrogen consumption during the complete mineralization of biomass was $1.56 \text{ mg of O}_2/\text{mg}$ of microcolonies and 0.15 mg of N/mg of microcolonies, respectively (Bailey

and Ollis, 1986). For the simulations, the model, MODFLOW, was run for the unsteady condition flow. The SEAM3D model, meanwhile, was used for the fate and biodegradation of hydrocarbon. The stress period to simulate the flow and transport and biodegradation on the beach was six months.

Eight scenarios were simulated to investigate the effect of tide amplitude and beach properties (i.e., longitudinal dispersivity, hydraulic conductivity). The parameter values of each scenario are shown in Table 1, where scenario 1 is considered the base case. The properties of each of the eight scenarios considered are summarized in Table 2. Table 3 shows the microbial parameters used in the numerical model.

3 Results and discussion

3.1 Model validation

The experimental data reported by Chen et al. (1992) was run in the SEAM3D model for validation as well as for the purpose of predicting the aerobic biodegradation and transport of benzene. Chen et al. (1992), it should be noted, presented both experimental and simulation results for benzene transport and biodegradation in a water-saturated soil column with a continuous flow. In their study, fixed amounts of benzene (20 mg/L) and hydrogen peroxide (132.7 mg/L O) were released to the column, and benzene concentration samples were analyzed accordingly in the simulation. The porosity and longitudinal dispersivity were found to be 0.38 and

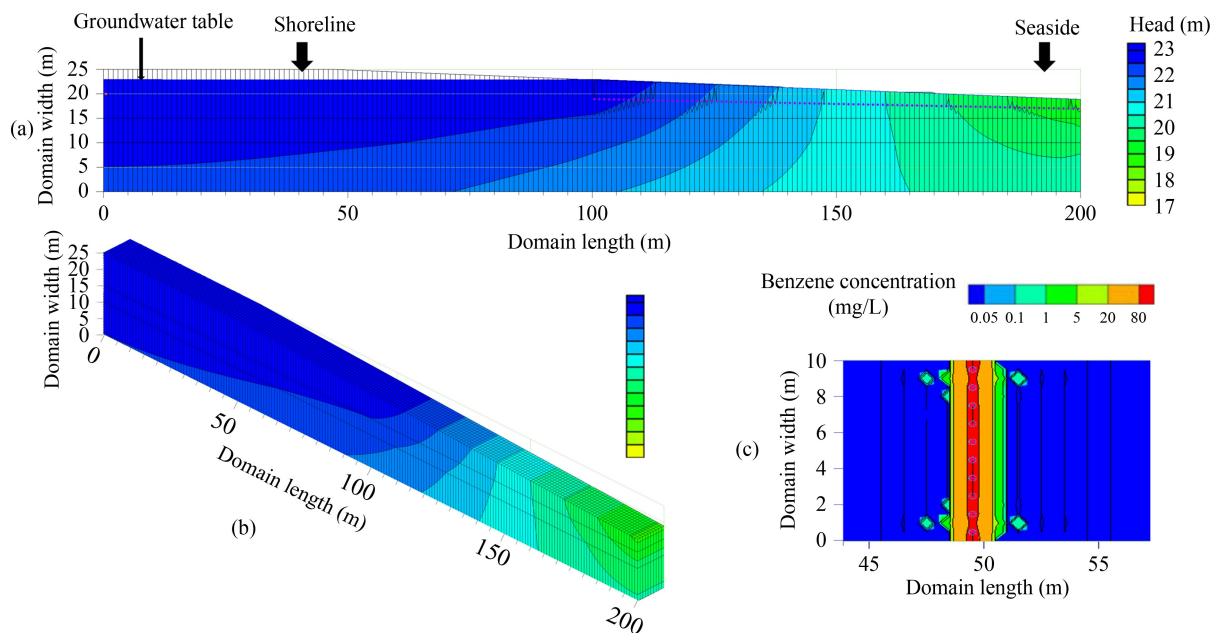


Fig. 1 (a) The front view of the model grid. The leaking location is 110 m from the seaside and 50 m in the shoreline, and the groundwater table is 2 m below the surface. (b) The schematic diagram of the three-dimensional model grid. (c) The plan view of the leaking location on $x = 50 \text{ m}$ with the contaminant concentration contours at $t = 0$.

0.0224 m, respectively. The kinetic parameter values were obtained from [Essaid et al. \(1995\)](#), who determined these values based on laboratory measurements and a literature review. These data have been used to validate various reactive solute transport models in past studies ([Essaid et al., 1995](#); [El-Kadi, 2001](#); [Ramakrishnan et al., 2015](#)).

[Figure 2](#) shows the experimental data, as well as the results achieved by the SEAM3D and those obtained by the models used in other studies ([Chen et al., 1992](#); [Essaid et al., 1995](#); [El-Kadi, 2001](#); [Geng et al. 2017](#)). It can be seen that the modeling with BIOMOC overpredicts benzene concentration. [Chen et al. \(1992\)](#) reported that the estimate of benzene degrader biomass underpredicted benzene concentrations. Therefore, the difference in the model and experimental data remains within the range of uncertainty in the model parameter evaluation. SEAM3D is able to delineate the subsurface transport of various solutes in a 3D, anisotropic, heterogeneous region subject to advection, dispersion, adsorption, and biodegradation. This model can be used to simulate complicated biodegradation problems such as multiple substrates and multiple electron acceptors. As shown in the figure, the SEAM3D model has been proven effective in representing the aerobic biodegradation and transport of benzene in the soil column.

3.2 Groundwater flow distribution

In this study, groundwater flowed vertically downward through the three-dimensional model grid. In the base scenario, the tide amplitude was 1 m and the upper hydraulic head changed with time in a range of 19 to 22 m. In other scenarios, the tide amplitude changed to 2 and 3 m, with the maximum hydraulic head of 23 and 24 m, respectively. The hydraulic head of the upper boundary on the seaside changed with time in different scenarios due to the tide effect, thus resulting in transient groundwater flow in terms of magnitude and flow direction.

[Figure 3](#) shows the groundwater flow and velocity fields in response to different tide levels when the tide was under the highest condition. In particular, [Fig. 3\(a\)](#) shows the model contours and the velocity magnitude of transient flow in the no-tide state; as can be seen, terrestrial groundwater flow discharged from the beach to the sea near the intersection between the shoreline and mean sea level. The flow moved from the shoreline (with higher groundwater level on the left side) toward the seaside and discharged into the sea. [Figure 3\(b\)](#) illustrates the flow condition with a tide amplitude of 1 m and tide exposure about 30 m toward the beach. As the tide amplitude increased, so did the span of the intertidal zone, as shown in [Figs. 3\(c\) and 3\(d\)](#); the tide exposure for tide amplitudes of 2 and 3 m were 60 and 90 m, respectively. In shorelines, there is the interaction between groundwater and nearshore sea water. As the tide comes,

Table 1 Characteristics of the numerical experiments and different scenarios that are analyzed in this study

Scenario	Tide amplitude (m)	Longitudinal dispersivity (m)	Hydraulic conductivity (m/h)
1	1	0.3	1.8
2	2	0.3	1.8
3	3	0.3	1.8
4	0	0.3	1.8
5	1	0.3	3.6
6	1	0.3	0.9
7	1	0.6	1.8
8	1	0.1	1.8

Table 2 Physical parameters used in the numerical simulations

Definition	Unit	Value
Porosity	/	0.3
Hydraulic conductivity	m/h	1.8
Specific storage	1/m	10^{-4}
Vertical anisotropy	/	10
Horizontal anisotropy	/	1
Longitudinal dispersivity	m	0.3

Table 3 Microbial parameters used in numerical model

Microbial properties	Units	Value
Distribution coefficient of benzene	m^3/g	3.6×10^{-8}
Initial mass fraction of benzene	/	0.05
Solubility of benzene	mg/L	1780
Inhibition coefficient of $\text{NO}_3\text{-O}_2$	g/m^3	0.6
Stoichiometric coefficient for oxygen consumption based on complete mineralization	mg of O_2 /mg of S	3.47
Stoichiometric coefficient for oxygen consumption during the complete mineralization of biomass	mg of O_2 /mg of X	1.56
Stoichiometric coefficient for nitrogen consumption during the complete mineralization of biomass	mg of N/mg of X	0.15
Dissolved rate	1/d	0.05

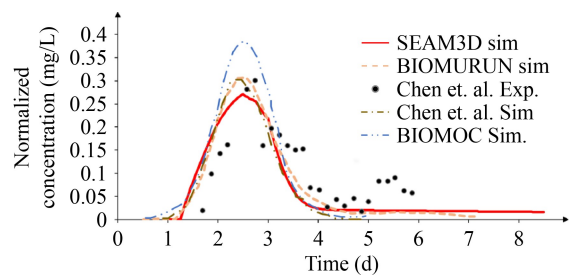


Fig. 2 Evaluated aerobic biodegradation of benzene and simulation results using SEAM3D and models developed by other studies ([Chen et al., 1992](#); [El-Kadi, 2001](#); [Essaid et al., 1995](#); [Geng et al., 2017](#)). The experimental results were reported in [Chen et al. \(1992\)](#).

the impacted flow may also result in the change of pollutant movement (Geng et al., 2015). At high tide condition, the groundwater table was elevated toward the shoreline side. Due to the tide effect, the front water affected the groundwater flow. Increasing the tide amplitude caused an increase in the intertidal zone and intrusion of the seawater to the groundwater, having an impact on the groundwater flow velocity and direction. The downward movement occurs with increasing tides, while the seaward flow occurs mainly as tides fall (Bhosale and Kumar, 2002).

3.3 Fate and transport of contaminants

Figure 4 shows the transport of the benzene plume and dissolved oxygen and nutrient concentrations on the beach 7, 30, and 90 d after the primary contaminant discharge. Due to the constant release in the first 15 d, the benzene plume extended around its source point, as shown in the figure. It is evident that the plume of contaminant was expanding in the seaward and downward directions due to the fact that the regional groundwater hydraulic gradient was in a seaward direction. Movement deeper into the beach both facilitated plume transport in the groundwater and caused greater expansion in the downward direction. After 15 d, the benzene release ceased, and the contaminant plume began to relocate and move seaward. As can be seen in the Fig. 4(a), the benzene plume concentration began to diminish at this juncture, since it had left its source point. This could be the result of dispersion in the surrounding groundwater and biodegradation.

The simulation shows that approximately 99% of benzene was biodegraded on the beach before being

released to the sea. Low oxygen and nutrient plumes were produced on the beach following the initial release of benzene due to biodegradation and associated microbial degradation. The oxygen reduction plume initially expanded around the source point of the contaminant and moved seaward, a behavior which is in line with the expected evolution of a benzene plume. The reduction of the oxygen and nutrient plumes, meanwhile, is due to the hydrocarbon biodegradation. Following the primary benzene discharge, bacteria degrade the benzene and convert it to biomass, carbon dioxide, and water. However, for aerobic biodegradation, the dissolved oxygen is required as an electron acceptor, and nutrients are needed for growth and for functions such as adenosine triphosphate (ATP) production. In fact, 3 g of oxygen is needed for 1 g of carbon to biodegrade. Therefore, the amount of oxygen required for biodegradation is greater than the number of nutrients required. Figure 4 illustrates that the low oxygen plume formed is considerably larger than the size of the nutrient consumption plume in the shoreline. Moreover, the model results show that natural degradation is a critical process as the contaminant plume migrates. Simultaneously, the dissolved oxygen conditions are a vital indicator for evaluating the fate of benzene.

3.4 Effects of the tide

Environmental conditions can often play an important role in the pollutant transport and fate (Ordieres-Meré et al., 2020; Shrestha and Wang, 2020). In the present study, four simulations were conducted with different tidal amplitudes ($A = 1, 2, 3,$ and 0 m) in order to investigate the effect of the tide on the fate and transport

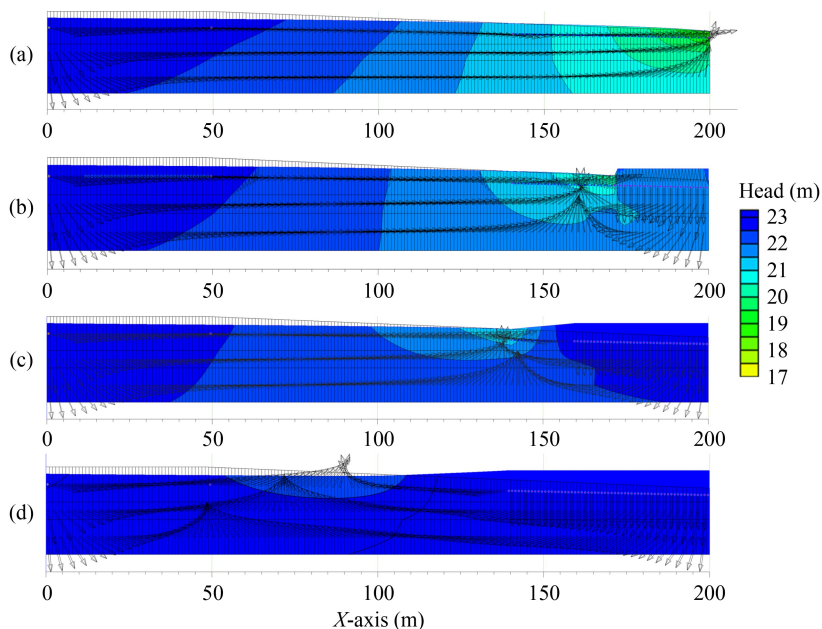


Fig. 3 Velocity vectors and flow condition. (a) Case 4 (no tide). (b) Case 1 ($A = 1$ m). (c) Case 2 ($A = 2$ m). (d) Case 3 ($A = 3$ m).

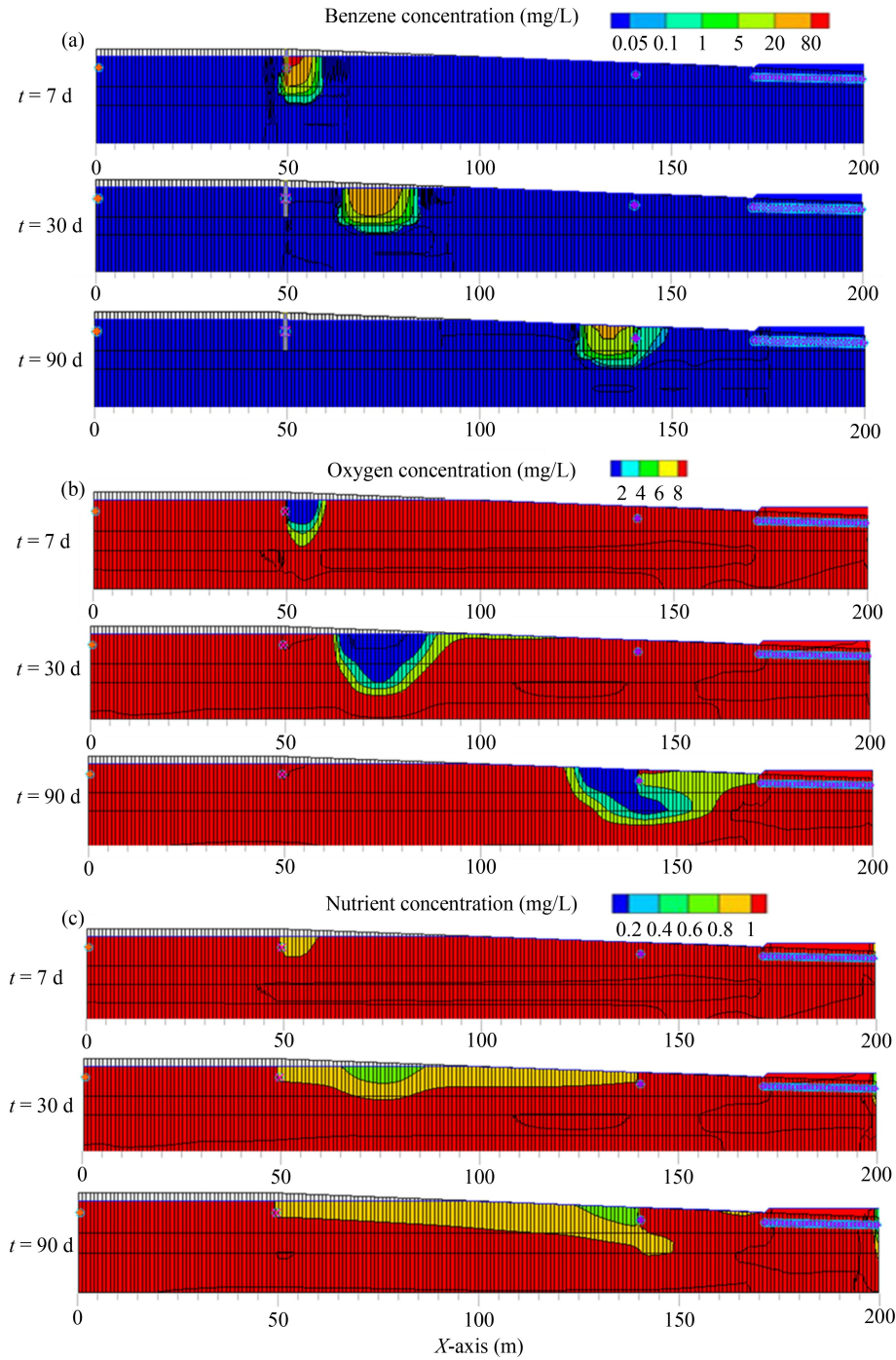


Fig. 4 Concentration contour in base scenario ($A = 1$). (a) Fate and transport of the benzene after 7, 30 and 90 d. (b) Oxygen consume due to microbial degradation after 7, 30 and 90 d. (c) Nutrient concentration in domain after 7, 30 and 90 d.

of contaminants in the beach. As shown in Table 1, case 1 ($A = 1$) is considered the base case with which the other cases are compared. Figure 5 reports the concentration of benzene (mg/L) in relation to time (d) in different locations. As mentioned above, the point source location is at $x = 50$ m. Figure 5(a) illustrates the concentration of benzene after 40 d at $x = 60$ m (10 m after the release position), while Figs. 5(b) and 5(c) represent the concentration of benzene at $x = 130$ m (80 m downwards

from the benzene point source location in the saturated zone).

Figure 5(a) shows that the plume reached this location ($x = 60$ m) in cases 1, 2, and 4 with the tide amplitude of 1 m, 2 m, and no tide, whereas in case 3 (tide amplitude = 3 m) the benzene plume was transported 10 m from the point source location with a lag of approximately two days. The figure shows that the benzene concentration was affected by the tide amplitude, as well. For instance,

the concentration of benzene in case 3 ($A = 3$) is almost 10 mg/L less than that in the base case, signaling greater plume dispersion and chemical reaction than in the base case. The maximum concentration transport of benzene in cases 2 and 3, meanwhile, is almost the same as in case 1. As shown in Fig. 3, the tidal zone was different in each case; in cases 1 and 2, the tidal zone was 120 and 110 m, respectively, from the point source release, while in case 3, the tidal zone was 90 m from the source, meaning that the effect of tide amplitude in case 3 was more significant.

Figures 5(b) and 5(c) represent the benzene concen-

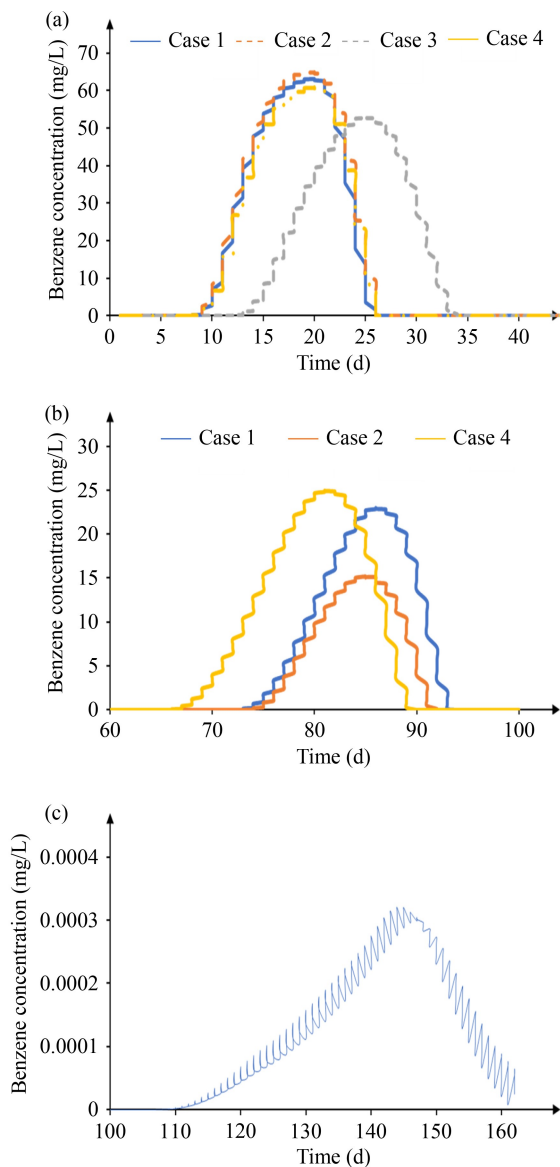


Fig. 5 Tide effect on the concentration of benzene in time at a different location: (a) Tide effect on different scenarios (Case 1, 2, 3 and 4) at $x = 60$ m (10 m after source point), (b) Tide effect on case 1, 2, 4 at $x = 130$ (80 m after the benzene release source), (c) Benzene concentration at $x = 130$ for case 3 (due to the small amount of benzene concentration in this location the graph has been shown separately).

tration in relation to time at the point 80 m from the benzene release and 70 m from the seaside. It can be seen that, in case 1 ($A = 1$ m), 22% of the benzene reached this location, while this proportion is 15% for case 2 ($A = 2$ m), 0.00033% for case 3 ($A = 3$), and 25% for case 4 (no tide). It was also found that approximately 99% of the benzene was biodegraded on the beach before being released into the sea. The results show that 30% of the benzene released was biodegraded within 10 m of the release point and almost 70% within 80 m. Figure 5(c) shows that the tide tended to augment the dispersion and chemical reaction effects on the plume; accordingly, the amount of benzene that reached point $x = 130$ m was very small compared to other situations. A higher tide amplitude served to enhance the seawater infiltration and mixing between oxygen-rich seawater and benzene-contaminated groundwater, leading to faster biodegradation and larger dispersion of the benzene plume. Since the tidal zone started at 140 m in case 3, the effect of the tide was significant.

Figure 6 shows the spreading area of the plume after releasing benzene under different tide amplitude conditions. As the tide amplitude increased, the spreading area shrank, and this effect was more pronounced in case 3 due to the high tide amplitude and the zone affected by the tide. In cases 1, 2, and 4, the benzene plume spread approximately 180 to 200 m, while in case 3, the benzene plume extended just 110 m. It is shown that when the tide amplitude increased, the span of the intertidal zone increased. With a 1 m tide amplitude, the tide exposure was about 30 m toward the beach, while the distances were 60 and 90 m for a tide amplitude of 2 and 3 m, respectively. At high-tide conditions, the groundwater table was elevated toward the shoreline side.

In this study, it should be noted, our focus is on tidally-influenced aquifer systems of either freshwater or saltwater (but not a combination of both), and therefore density effects and associated freshwater–saltwater mixing are not considered. Density gradients generated by the mixing of terrestrial fresh groundwater and seawater have been found to have a significant effect on nearshore flow and transport processes. Although the density difference between seawater and terrestrial freshwater is an important consideration in most aquifer systems, there are numerous scenarios in which the density effects are negligible. For example, saltwater can intrude inland a long distance in coastal aquifers. In addition, pore water salinity in tidal freshwater marshes can be low and, therefore, density gradients are negligible in these tidally-influenced aquifer systems. The findings of the present study are applicable to such scenarios.

3.5 Effects of hydraulic conductivity

Different scenarios were simulated to investigate the

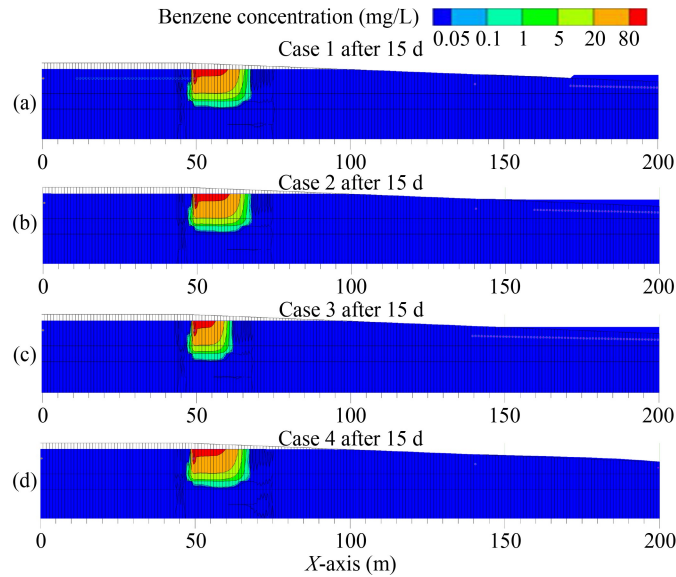


Fig. 6 Spreading area of the benzene plume after 15 d affected by different tide amplitude for the first scenario; the area shrinks due to an increase in the tide amplitude.

effect of various beach characteristics on plume transport and fate. Various properties, such as hydraulic conductivity, specific storage, and specific yield, can affect plume transport (Bear and Cheng, 2010; Kheirandish et al., 2020). The sensitivity analysis shows that the simulation model was most sensitive to hydraulic conductivity changes among these properties. As such, in this section, hydraulic conductivity changes and the corresponding effect on benzene transport are discussed. Hydraulic conductivity, it should be noted, describes the ability of the soil to transfer fluid through voids. The hydraulic conductivity range for the coastal aquifer can be from 0.049 to 8.09 m/h (Lathashri and Mahesha, 2016). As Table 1 shows, cases 5 and 6 had different hydraulic conductivities (3.6 and 0.9 m/h, respectively). To better understand the effect of hydraulic conductivity, these two cases were compared to case 1 (1.8 m/h), as shown in Fig. 7. Figure 7(a) represents the effect of different hydraulic conductivities on the amount of benzene transport 10 m after point source and the associated time lag for plume transport.

The results show that, in the base case (case 1), 60% of the benzene reached the point $x = 60$ m after 20 d. In comparison, the maximum concentrations transferred to this point in cases 5 and 6 were 66 mg/L (after 17 d) and 41 mg/L (after 27 d), respectively. Figures 7(b) and 7(c) show the benzene concentration that reached the saturated zone ($x = 130$ m) after a specific time in different situations. In case 1, approximately 80% of the benzene was biodegraded before reaching this point. In contrast, this proportion was 50% for case 5 and 99% for case 6. The diagrams also show that, on the beach with more permeable sediment, the plume transport was faster and, as such, the microbial degradation benzene's of was lower. Due to the low hydraulic conductivity in this case, the plume moved more slowly, meaning that the

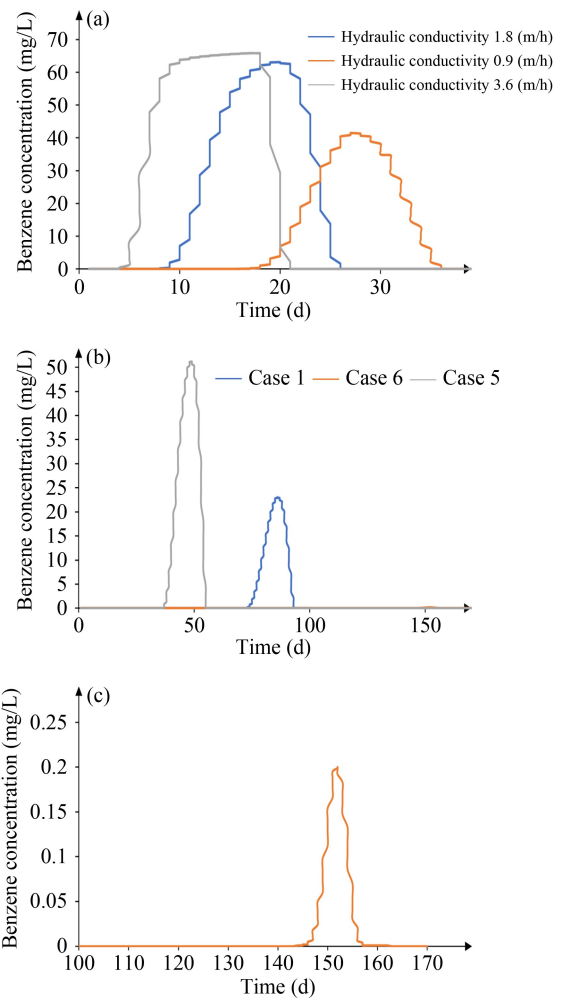


Fig. 7 Effect of hydraulic conductivity on plume concentration during the specific time: (a) concentration versus time at $x = 60$ m (10 m after benzene released). (b) and (c) plume concentration versus time at $x = 130$ (80 m after point source).

contaminant's residence time on the beach was longer, and the plume had a longer resistance to degrade at each part of the beach. In case 6, due to the longer residence time at the $x = 60$ m zone and adequate oxygen replenishment, a greater portion of the contaminant was biodegraded along its pathways than in case 5. The significant goal for successful bioremediation is to maximize the oil's residence time on the beach and hence its contact with microorganisms (Boufadel et al., 2006).

Figure 8 demonstrates that hydraulic conductivity affects the plume expansion significantly. As shown in Fig. 8(a) with respect to case 6, the plume expansion was minimal after 30 d and was still in the unsaturated zone. As shown in Fig. 8(c) with respect to case 5, in contrast, the plume expansion was greater, and it reached the saturated zone. These results indicate that hydraulic conductivity is an important consideration when assessing the resistance of pollution on coastal beaches. The simulation results also demonstrate that hydraulic conductivity can considerably affect the plume degradation rate at various parts of the shoreline.

3.6 Effect of longitudinal dispersivity

Longitudinal dispersivity is one of the main beach properties that may affect the plume transport and fate. Therefore, in this research, two cases were considered in order to observe the consequences of longitudinal dispersivity changes. Fluid does not move at uniform velocity throughout the soil; instead, mixing occurs along flow paths in a phenomenon known as longitudinal dispersion. Longitudinal dispersivity values obtained from experiments and simulations range from 0.07 to 11 m for different kinds of sandy aquifers (Schulze - Makuch, 2005). As shown in Table 1, cases 7 and 8 had

different longitudinal dispersivities—0.6 m and 0.1 m, respectively—compared to case 1 (0.3 m). Figure 9(a) shows the simulation results of cases 1, 7, and 8 at point $x = 60$ m (10 m after benzene release), while Fig. 9(b) shows the results when the plume passed 80 m into the beach (i.e., $x = 130$ m). The results show that the maximum plume concentration was reached at point $x = 60$ m in approximately 20 days in all cases.

Figure 9(a) indicates that about 63% of the benzene released in the groundwater reached $x = 60$ m in case 1, while this proportion was 59.5% for case 7 and 64% for case 8. The results for different longitudinal dispersivity cases 80 m after point source are shown in Fig. 9(b). As can be seen, by the time the longitudinal dispersivity doubled, 88% of the benzene had dispersed and biodegraded along its flow path. In comparison, this proportion was about 77% in the base case and 60% when the longitudinal dispersivity was 0.1 m. The simulation results illustrate that changing the longitudinal dispersivity does not significantly affect the plume duration transport, while it does considerably affect the concentration of benzene. In other words, the plume disperses and biodegrades during its transport, causing a reduction in the contaminant concentration. Therefore, when the longitudinal dispersivity increases, so does the dispersion, and the benzene concentration decreases accordingly.

4 Conclusions

The research presents the numerical simulation of benzene transport in shoreline groundwater affected by tides under different conditions. First, on tide-influenced beaches, aerobic biodegradation plays a significant role in

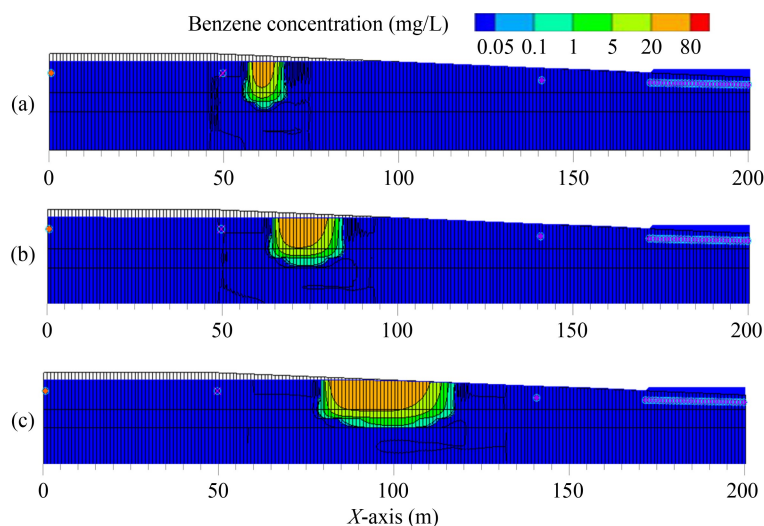


Fig. 8 Plume transport after 30 d. (a) Hydraulic conductivity 0.9 m/h (case 6). (b) Hydraulic conductivity 1.8 m/h (case 1). (c) Hydraulic conductivity 3.6 m/h (case 5).

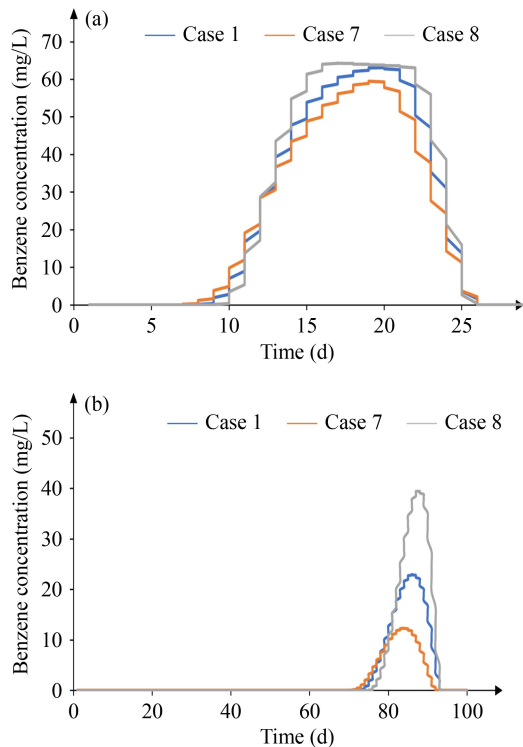


Fig. 9 Effect of longitudinal dispersivity on benzene concentration during the time. (a) Concentration of benzene 10 m after the point source. (b) Concentration of benzene 80 m after releasing contaminant.

plume transport and benzene fate, particularly when the point source is far from the sea zone. In microbial biodegradation, a large amount of oxygen is required, so a low-oxygen plume emerges in the groundwater. Second, benzene released into the groundwater is found to biodegrade up to 70% in beach aquifers, meaning that 30% of the initial benzene release is discharged into the ocean. Third, an increase in tide amplitude serves to augment the microbial biodegradation due to the significant increase in the plume's residence time. Moreover, a higher tide amplitude makes the contaminant plume smaller and reduces the spreading area of the pollution. Fourth, hydraulic conductivity has an enormous impact on the biodegradation rate in beach groundwater. Finally, longitudinal dispersivity also affects the concentration of benzene passing through its flow path to the sea without biodegrading. These results can be used to support future risk assessment and management for the shorelines impacted by spill and leaking accidents.

Acknowledgements This research was supported by the Multi-partner Research Initiative of Fisheries and Oceans Canada and the Natural Sciences and Engineering Research Council of Canada. The authors are particularly thankful to the comments and suggestions from international experts of oil spill control and response. The authors are also grateful to Huifang Bi, the editor and the anonymous reviewers for their insightful comments and suggestions.

References

- Anderson M P, Woessner W W, Hunt R J (2015). Applied groundwater modeling: Simulation of flow and advective transport, 2nd ed. New York: Elsevier
- Asif Z, Chen Z (2020). A life cycle based air quality modeling and decision support system (LCAQMS) for sustainable mining management. *Journal of Environmental Informatics*, 35(2): 103–117
- Atlas R M, Hazen T C (2011). Oil biodegradation and bioremediation: A tale of the two worst spills in US history. *Environmental Science & Technology*, 45(16): 6709–6715
- Babamiri O, Vanaei A, Guo X, Wu P, Richter A, Ng K T W (2021). Numerical simulation of water quality and self-purification in a mountainous river using QUAL2KW. *Journal of Environmental Informatics*, 37(1): 26–35
- Bailey J, Ollis D (1986). *Biochemical engineering fundamentals*. New York: McGraw-Hill
- Bear J, Cheng A H D (2010). *Modeling groundwater flow and contaminant transport* (Vol. 23). Springer Science & Business Media
- Bhosale D, Kumar C (2002) Simulation of seawater intrusion in Ernakulam coast. In: *Proceedings of International Conference on Hydrology and Watershed Management, Hyderabad*, 390–399
- Bi H, An C, Chen X, Owens E, Lee K (2020). Investigation into the oil removal from sand using a surface washing agent under different environmental conditions. *Journal of Environmental Management*, 275: 111232
- Boufadel M C, Geng X, Short J (2016). Bioremediation of the Exxon Valdez oil in Prince William sound beaches. *Marine Pollution Bulletin*, 113(1–2): 156–164
- Boufadel M C, Suidan M T, Venosa A D (1999). A numerical model for density-and-viscosity-dependent flows in two-dimensional variably saturated porous media. *Journal of Contaminant Hydrology*, 37(1–2): 1–20
- Boufadel M C, Suidan M T, Venosa A D (2006). Tracer studies in laboratory beach simulating tidal influences. *Journal of Environmental Engineering*, 132(6): 616–623
- Brock T D, Madigan M T, Martinko, J M, Parker J (2003). *Biology of microorganisms*, 10th ed. New Jersey: Prentice Hall
- Brovelli A, Mao X, Barry D (2007). Numerical modeling of tidal influence on density-dependent contaminant transport. *Water Resources Research*, 43(10): W10426
- Chen Y M, Abriola L M, Alvarez P J, Anid P J, Vogel T M (1992). Modeling transport and biodegradation of benzene and toluene in sandy aquifer material: Comparisons with experimental measurements. *Water Resources Research*, 28(7): 1833–1847
- Chen Z K, An C, Boufadel M C, Owens E, Chen Z, Lee K, Cao Y, Cai M (2020). Use of surface-washing agents for the treatment of oiled shorelines: Research advancements, technical applications and future challenges. *Chemical Engineering Journal*, 391: 123565
- Colombani N, Mastrocicco M, Prommer H, Sbarbati C, Petitta M (2015). Fate of arsenic, phosphate and ammonium plumes in a coastal aquifer affected by saltwater intrusion. *Journal of Contaminant Hydrology*, 179: 116–131

- El-Kadi A I (2001). Modeling hydrocarbon biodegradation in tidal aquifers with water-saturation and heat inhibition effects. *Journal of Contaminant Hydrology*, 51(1–2): 97–125
- Essaid H I, Bekins B A, Godsy E M, Warren E, Baedecker M J, Cozzarelli I M (1995). Simulation of aerobic and anaerobic biodegradation processes at a crude oil spill site. *Water Resources Research*, 31(12): 3309–3327
- Essaid H I, Cozzarelli I M, Eganhouse R P, Herkelrath W N, Bekins B A, Delin G N (2003). Inverse modeling of BTEX dissolution and biodegradation at the Bemidji, MN crude-oil spill site. *Journal of Contaminant Hydrology*, 67(1–4): 269–299
- Geng X, Boufadel M C, Cui F (2017). Numerical modeling of subsurface release and fate of benzene and toluene in coastal aquifers subjected to tides. *Journal of Hydrology (Amsterdam)*, 551: 793–803
- Geng X, Boufadel M C, Lee K, Abrams S, Suidan M (2015). Biodegradation of subsurface oil in a tidally influenced sand beach: Impact of hydraulics and interaction with pore water chemistry. *Water Resources Research*, 51(5): 3193–3218
- Geng X, Boufadel MC, Lee K, An C (2020a). Characterization of pore water flow in 3-D heterogeneous permeability fields. *Geophys Res Lett*, 47(3): e2019GL086879
- Geng X, Michael HA, Boufadel MC, Molz FJ, Gerges F, Lee K (2020b) Heterogeneity affects intertidal flow topology in coastal beach aquifers. *Geophys Res Lett*, 47(17): e2020GL089612
- He L, Li Y, Zhu F, Sun X, Herrmann H, Schaefer T, Zhang Q, Wang S (2020). Insight into the mechanism of the OH-induced reaction of ketoprofen: A combined DFT simulation and experimental study. *Journal of Environmental Informatics*, 35(2): 128–137
- Heiss J (2011). Intertidal mixing zone dynamics and swash induced infiltration in a sandy beach aquifer, Cape Henlopen, Delaware. Dissertation for the Ph. D Degree Delaware: University of Delaware
- Heiss J, Michael H A (2014). Saltwater-freshwater mixing dynamics in a sandy beach aquifer over tidal, spring-neap, and seasonal cycles. *Water Resources Research*, 50(8): 6747–6766
- Jiang Y, Xi B, Li R, Li M, Xu Z, Yang Y, Gao S (2019). Advances in Fe(III) bioreduction and its application prospect for groundwater remediation: A review. *Frontiers of Environmental Science & Engineering*, 13(6): 89
- Khaska M, Le Gal La Salle C, Lancelot J, team A S T E R, Mohamad A, Verdoux P, Noret A, Simler R (2013). Origin of groundwater salinity (current seawater vs. saline deep water) in a coastal karst aquifer based on Sr and Cl isotopes. Case study of the La Clape massif (southern France). *Applied Geochemistry*, 37: 212–227
- Kheirandish M, Rahimi H, Kamaliardakani M, Salim R (2020). Obtaining the effect of sewage network on groundwater quality using MT3DMS code: Case study on Bojnourd plain. *Groundwater for Sustainable Development*, 11: 100439
- Lathashri U, Mahesha A (2016). Predictive simulation of seawater intrusion in a tropical coastal aquifer. *Journal of Environmental Engineering*, 142(12): D4015001
- Leahy J G, Colwell R R (1990). Microbial degradation of hydrocarbons in the environment. *Microbiology and Molecular Biology Reviews*, 54(3): 305–315
- Lee K, Boufadel M C, Chen B, Foght J, Hodson P, Swanson S, Venosa A (2015). Expert panel report on the behaviour and environmental impacts of crude oil released into aqueous environments. Royal Society of Canada, Ottawa: ON
- Li C, Yan L, Li Y, Zhang D, Bao M, Dong L (2021). TiO₂@palygorskite composite for the efficient remediation of oil spills via a dispersion-photodegradation synergy. *Frontiers of Environmental Science & Engineering*, 15(4): 72
- Li H, Boufadel M C (2010). Long-term persistence of oil from the Exxon Valdez spill in two-layer beaches. *Nature Geoscience*, 3(2): 96–99
- Liu Y, Jiao J J, Luo X (2016). Effects of inland water level oscillation on groundwater dynamics and land-sourced solute transport in a coastal aquifer. *Coastal Engineering*, 114: 347–360
- Liu Z, Liu J, Zhu Q, Wu W (2012). The weathering of oil after the Deepwater Horizon oil spill: Insights from the chemical composition of the oil from the sea surface, salt marshes and sediments. *Environmental Research Letters*, 7(3): 035302
- Lu G, Clement T P, Zheng C, Wiedemeier T H (1999). Natural attenuation of BTEX compounds: Model development and field-scale application. *Ground Water*, 37(5): 707–717
- Mehl S W, Hill M C (2001). User guide to the Link-AMG (LMG) package for solving matrix equations using an algebraic multigrid solver. U.S. Geological Survey Open File Report 01–177. Reston. USGS: Virginia
- Ordieres-Meré J, Ouarzazi J, El Johra B, Gong B (2020). Predicting ground level ozone in Marrakesh by machine-learning techniques. *Journal of Environmental Informatics*, 36(2): 93–106
- Ramakrishnan A, Blaney L, Kao J, Tyagi R D, Zhang T C, Surampalli R Y (2015). Emerging contaminants in landfill leachate and their sustainable management. *Environmental Earth Sciences*, 73(3): 1357–1368
- Robinson C, Gibbes B, Carey H, Li L (2007). Salt-freshwater dynamics in a subterranean estuary over a spring-neap tidal cycle. *Journal of Geophysical Research*, 112(C9): C09007
- Santos F, DeCastro M, Gómez-Gesteira M, Álvarez I (2012). Differences in coastal and oceanic SST warming rates along the Canary upwelling ecosystem from 1982 to 2010. *Continental Shelf Research*, 47: 1–6
- Sbarbati C, Colombani N, Mastrocicco M, Aravena R, Petitta M (2015). Performance of different assessment methods to evaluate contaminant sources and fate in a coastal aquifer. *Environmental Science and Pollution Research International*, 22(20): 15536–15548
- Schulze-Makuch D (2005). Longitudinal dispersivity data and implications for scaling behavior. *Ground Water*, 43(3): 443–456
- Shrestha N, Wang J (2020). Water quality management of a cold climate region watershed in changing climate. *Journal of Environmental Informatics*, 35(1): 56–80
- Torlapati J, Boufadel M C (2014). Evaluation of the biodegradation of Alaska North Slope oil in microcosms using the biodegradation model BIOB. *Frontiers in Microbiology*, 5: 212
- Uraizee F A, Venosa A D, Suidan M T (1997). A model for diffusion controlled bioavailability of crude oil components. *Biodegradation*, 8(5): 287–296
- Wang Z, An C, Chen X, Lee K, Zhang B, Feng Q (2021). Disposable masks release microplastics to the aqueous environment with exacerbation by natural weathering. *Journal of Hazardous Materials*, 417: 126036

- Widdowson M A, Molz F J, Benefield L D (1988). A numerical transport model for oxygen-and nitrate-based respiration linked to substrate and nutrient availability in porous media. *Water Resources Research*, 24(9): 1553–1565
- Xu Z, Chai J, Wu Y, Qin R (2015). Transport and biodegradation modeling of gasoline spills in soil-aquifer system. *Environmental Earth Sciences*, 74(4): 2871–2882
- Zhai A, Ding X, Liu L, Zhu Q, Huang G (2020a). Total phosphorus accident pollution and emergency response study based on geographic information system in Three Gorges Reservoir area. *Frontiers of Environmental Science & Engineering*, 14(3): 46
- Zhai A, Ding X, Zhao Y, Xiao W, Lu B (2020b). Improvement of instantaneous point source model for simulating radionuclide diffusion in oceans under nuclear power plant accidents. *Journal of Environmental Informatics*, 36(2): 133–145
- Zhao Y, Lin L, Hong M (2019). Nitrobenzene contamination of groundwater in a petrochemical industry site. *Frontiers of Environmental Science & Engineering*, 13(2): 29